ORIGINAL ARTICLE

Development of an enhanced damage law for typical steel fiber reinforced concrete based on uniaxial compression and tension tests

Sören Faustmann · **Andreas Wolf** ·
Oliver Fischer

Abstract Understanding the stiffness of a concrete structure is crucial to analyze it, particularly for statically indeterminate structures. Stiffness degradation – commonly referred to as damage – occurs with the onset of cracking or large compressive strains. For most conventional and specialized types of concrete, damage studies and models for predicting damage development are available. However, more information is needed about the damage behavior for the most common steel fiber reinforced concrete in Europe with strength class C30/37 and modern end-anchored high-strength fibers in dosages of 20–40 kg/m³. Therefore, in this study, these common steel fiber concretes were subjected to multiple load cycles in (1) uniaxial compression tests on cylinders and (2) direct tensile tests on bone specimens to investigate their damage behavior. The resulting damage was then compared to known damage laws, but none of the models predicted accurate damage results. Finally, an existing damage law for plain concrete was modified as a function of the residual flexural tensile strength—the relevant parameter for describing the performance of the steel fiber reinforced concrete. Hereby, we were able to decisively improve the agreement between experimental results and the theoretical prognosis by utilizing our modified damage law.

1 Introduction

Steel fiber reinforced concrete (SFRC) for structural applications is more commonly used, which is reflected for instance by the inclusion of SFRC in the new Eurocode 2 [1]. Realistic prediction models, e.g. based on numerical simulations [2–4], require detailed knowledge of the material properties of SFRC. In addition to knowing the compressive and tensile properties, the stiffness degradation, also known as damage, at compressive strains or tensile cracks must be understood. Damage changes the stiffness ratios in the structure, resulting in a redistribution of internal forces in statically indeterminate systems. Accurate knowledge of damage processes is therefore essential for structural calculations. Damage can be determined experimentally using uniaxial low cycle tests. For plain concrete, such tests have already been carried out many times (e.g. compression tests in [5–7], tensile tests in [8–11]). This resulted in several approaches to calculate damage in compression

S. Faustmann (✉) · A. Wolf · O. Fischer
Chair of Concrete Structures, Technical University
of Munich, Theresienstraße 90, 80333 Munich, Germany
e-mail: soeren.faustmann@tum.de

O. Fischer
e-mail: oliver.fischer@tum.de

rilem

(e.g. [5, 6, 12–14]), and tension (e.g. [12, 13]). Dabbagh has listed further models in [15]. For other types of concretes, such as hybrid fiber reinforced concretes (HFRC) (e.g. [16, 17]), short polypropylene fiber enhanced recycled concrete (PFRAC) [18], and utrahigh-performance fiber-reinforced concrete (UHP-FRC) (e.g. [19]), there are also investigations and damage prediction models.

In the last few years, SFRC damage behavior studies have often been performed on flexural tensile tests [20–24]. However, they only allow indirect conclusions about the tensile damage behavior. There are also some studies on the uniaxial damage behavior of steel fibers under pure compression [25, 26] and tension [27–29]. The focus of these studies is on acoustic emission based damage monitoring [29], concretes with high compressive strength (f_c between 55 and 85 N/mm^2 [25, 29]) and steel fiber contents of 80–160 kg/m^3 [16, 26]. This far exceeds the commonly used steel fiber concretes with compressive strength classes ranging from C20/25 to C35/45 and fiber contents of 20–40 kg/m^3 [30], which are also investigated in other contexts in recent studies such as [21, 29, 31]. For those typical SFRCs, the authors are not aware of any low cyclic uniaxial investigation providing a quantification of the stiffness degradation (damage). For this reason, we have conducted and evaluated our own experimental investigation. The damage thus determined is compared with existing damage laws, and due to lack of agreement, we formulated a new (i.e. modified) relationship based on Marks damage law [12], also published in English language in [32].

2 Experiments

2.1 Materials

The concrete mix used was a C30/37 with a slightly increased w/c ratio to avoid excessively high strengths. The aim was to achieve a compressive strength of 35 N/mm^2 (Cylinder 150/300), which is in the lower to middle range of the C30/37 and therefore representative for typical SFRC [30]. Table 1 shows the concrete mix design. Dramix 4D 65/35 BG [33] steel fibers were used. These have 35 mm fiber length, 65 aspect ratio, 1,850 N/mm^2

Table 1 Concrete mix design

Cement CEM II/B-M 42,5 N (S-LL)	375 kg/m^3
Fly ash	40 kg/m^3
Sand 0–4 mm	802 kg/m^3
Gravel 4–8 mm	273 kg/m^3
Gravel 8–16 mm	632 kg/m^3
Water	199 kg/m^3
Superplasticizer FM Sika ViscoCrete 1095	0.64 kg/m^3
(w/c)$_{eq}$ regarding fly ash	0.51
Steel fibers Dramix 4D 65/35 BG [33]	varied content 80, 40 or 20 kg/m^3

nominal tensile strength, and 200,000 N/mm^2 nominal Young's modulus.

All tests were performed when the concrete was at least 28 days old. In addition to the actual tests, the fiber content was determined on three fresh concrete specimens (washout test) according to [34], three Young's modulus tests according to DIN EN 12390–13 [35], three-point flexural tests according to EN 14651 [36], and the residual flexural strengths f_{R1} to f_{R4} were evaluated. For the 4D80 and 4D40 fiber contents, the low-cycle compression and tensile tests were performed on different test days (i.e. different age if the specimens). A series of six flexural tests were performed on both test days. Due to the small deviation ≤ 0.5 N/mm^2 in the mean values per test day, all 12 tests per fiber content were averaged. The 4D20 tests were performed on one test day. Only one series of six flexural-tension tests was performed. Figure 1 shows the results of the flexural tests.

We evaluate the mean compressive strength of concrete from cylinder tests and derive the mean tensile strength from bone tests (see next section). Table 2 presents a summary of the principal material properties.

2.2 Test program and overview

The test program consisted of uniaxial compression tests on cylinders ($d/h = 150/300$ mm) and uniaxial tensile tests on bone shaped specimens. Table 3 shows the number of specimens tested. The series names all begin with 4D, which indicates the type of steel fiber used (Dramix 4D fibers), and a number following it
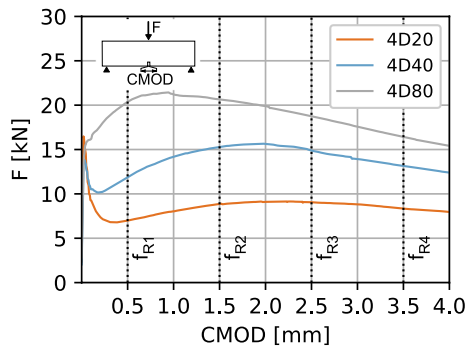
Fig. 1 Load-CMOD relations from three-point flexural tensile tests according to EN 14651 [36]

(20, 40, 80), indicating the steel fiber content in kg/m³.

Figure 2 shows the compression test setup. The cylinders were ground and the achieved flatness of the surfaces was checked. They were then tested in a 10 MN universal test rig, with strains and deformations of the specimen being recorded by three strain gauges and three linear variable differential transformers (LVDT's). To evaluate the compressive strain, the average of the three strain gauges was used until the peak load was reached. After the peak load, the strain was calculated as the average of the LVDT's divided by the height of the specimen. This procedure eliminates slip effects and has also been used by Müller in [38].

The load was applied in a displacement controlled manner in accordance with the scheme shown in Fig. 2c. The cylinders were unloaded in 0.30 mm increments to a very low load of 5 kN. The load was then reapplied under displacement control. The tests were continued until there was no longer significant

load that could be absorbed by the concrete. This resulted in 11 to 16 cycles per cylinder.

The setup of the direct tensile tests is shown in Fig. 3. After reviewing numerous specimen shapes and test setups in literature (e.g. [39–43]), we have chosen a 72 cm long bone with a width of 10 cm in the central region according to Look [42]. Half of the bone specimens were produced with bone-shaped formwork. For the remaining specimens, the bone shape was cut out of rectangular concrete prisms using a high-pressure water jet (analogous to Look [42]), which eliminates the lateral influence of fiber orientation at the edge of the formwork. No influence of the different manufacturing methods on the damage behavior was observed, therefore no differentiation is made in this paper.

The thickness of the bone specimens constantly is 10 cm. At each bone end, four M8 threaded rods cast in concrete with screwed-on nuts connected the bone to the test rig. The cross-sectional area of the bone tapers gradually without causing stress peaks [42, 43]. The crack is expected to occur in the central area marked in gray with a cross-sectional area of 100×100 mm. In the presented series of tests, this occurred in 27 of 29 bone specimens. Over this area, four LVDT's were placed to measure the developing crack opening. The reference length of the

Table 3 Number of specimens tested per series

Test series	4D20	4D40	4D80
Fiber content	20 kg/m³	40 kg/m³	80 kg/m³
No. of cylinders (compression)	6	6	6
No. of bone specimens (tension)	10	10	9

Table 2 SFRC material properties

V_f (kg/m³)	f_{cm} (N/mm²)	E_{c0} (N/mm²)	f_{ctm} (N/mm²)	f_{R1} (N/mm²)	f_{R2} (N/mm²)	f_{R3} (N/mm²)	f_{R4} (N/mm²)
80	34.8 COV = 3.8%	32,860*	2.41 COV = 11%	6.51 COV = 16%	6.61 COV = 15%	6.01 COV = 13%	5.25 COV = 15%
40	34.0 COV = 3.6%	33,462*	2.42 COV = 17%	3.80 COV = 19%	4.90 COV = 21%	4.77 COV = 21%	4.20 COV = 21%
20	35.4 COV = 1.9%	31,450*	2.83 COV = 8.1%	2.24 COV = 25%	2.84 COV = 25%	2.90 COV = 25%	2.67 COV = 25%

*Calculated according to Model Code 1990 [37] with formula: $E_{c0} = 2.15 \cdot 10{,}000 \cdot (f_{cm}/10)^{1/3}$

Fig. 2 Compression tests on cylinders: **a** test setup, **b** measurement equipment and **c** test program
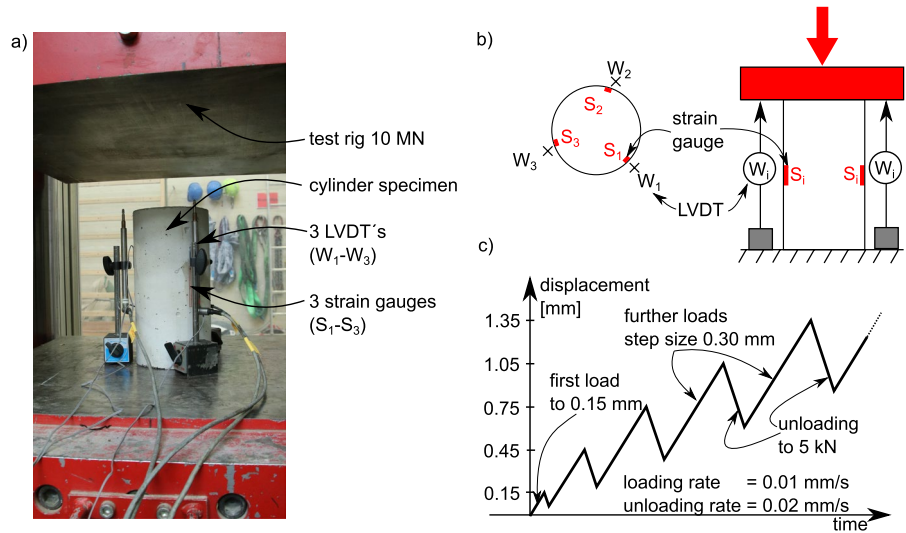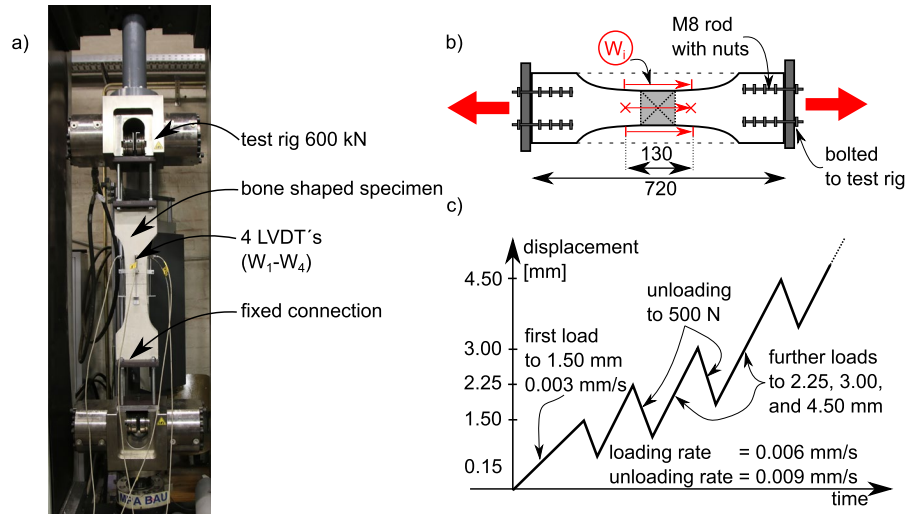

Fig. 3 Tensile tests on bone specimens **a** Test setup, **b** Measurement technique and load application, and **c** Test program

LVDT's was 130 mm. Up to a machine displacement of 1.50 mm, this was applied at a very slow rate of 0.003 mm/s. Within this loading step, a sudden initial cracking occurred, as can be also seen in [44]. After the initial crack appeared, the loading rate was increased to 0.006 mm/s. Each bone was unloaded to 500 N in four cycles at machine displacements of 1.50, 2.25, 3.00, and 4.50 mm.

2.3 Test results with a focus on damage

As the strain or crack opening increases, the stiffness of the SFRC decreases, which is typically referred to as damage. Figure 4a schematically shows the elements of plastic damage models that may be incorporated into FEM analyses, such as in the Concrete Damaged Plasticity model [45, 46]. At unloading, some components of the total strain (ε_c) are reversible (ε_{el}), while others remain as plastic strain (ε_{pl}). The Young's modulus decreases as the strain increases, which results in flatter gradients. Equation (1) can be used to calculate the damage parameter (d_c or d_t) if the actual modulus or gradient E_i is known. The same principles apply for tension, as shown in Fig. 4b.

$$d = 1 - \left(E_i / E_0 \right) \tag{1}$$

Fig. 4 Definition of stresses, strains, and damage under **a** compression, and **b** tension; modified from [12]
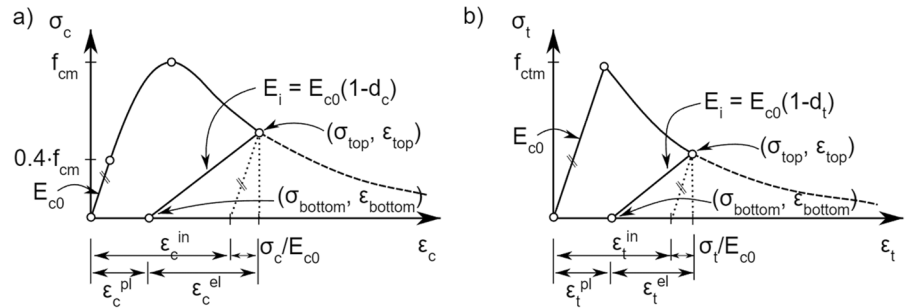

Figure 5 shows an example of the results of a single compression test 4D40_DV_01 with a steel fiber content of 40 kg/m³. In addition to the recorded stress–strain relationship including the unloading cycles, the peaks of the respective unloading cycles are marked with triangles and connected linearly. It can be clearly seen that these straight lines become flatter and flatter. The current modulus of elasticity E_i is determined from the difference of the strains according to Eq. (2).

$$E_i = \frac{\sigma_{\text{top}} - \sigma_{\text{bottom}}}{\varepsilon_{\text{top}} - \varepsilon_{\text{bottom}}} \qquad (2)$$

Equation 1 can then be used to determine the damage parameter d_c, which is plotted against the total strain in Fig. 5b. Each unloading cycle results in one marker in the damage diagram.

The same principle is applied in the tensile tests. Figure 6a shows the stress-crack width relationship of an exemplary test 4D40_ZZV_03, which has a fiber content of 40 kg/m³. There is no measurable crack width until the tensile strength of 2.72 N/mm² is reached. Subsequently, a crack with a width of approx. 0.5 mm develops suddenly and the steel fibers take over the load-bearing function. Here, too, the extreme points of the unloading loops are marked with triangles and linearly connected, allowing the current stiffness E_i to be calculated. Using Eq. 1, the relationship to the damage parameter d_t is also calculated here and plotted against the crack width in Fig. 6b. With four scheduled unloading cycles per bone, there are four markers in the damage diagram.

Figure 7 shows the damage values determined in this way as points of all individual tests sorted by test series 4D20, 4D40 and 4D80. Regression polynomials were calculated for each fiber content from all individual damage values, which are presented as solid lines. The root mean square error (RMSE) between each set of data points and the regression polynomial, which describes the average deviation in
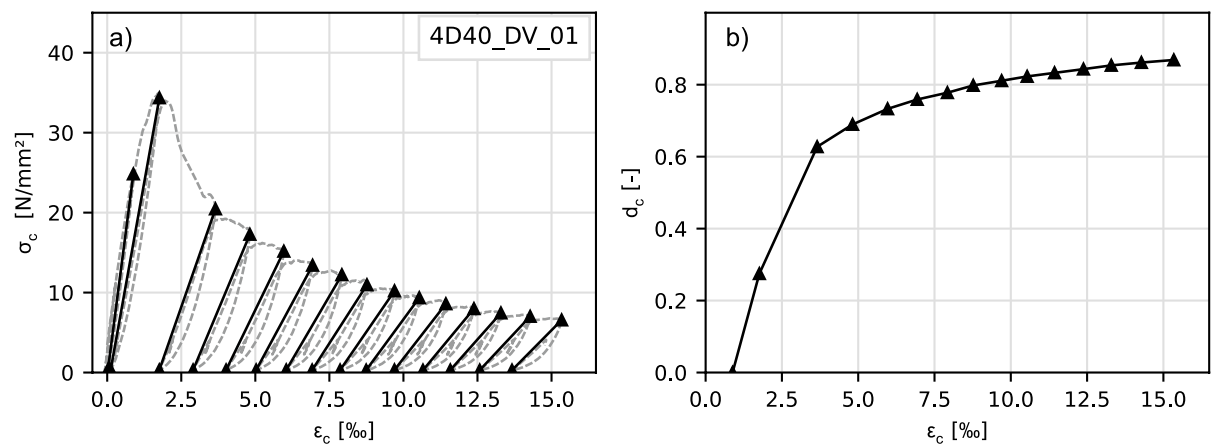

Fig. 5 Test result of a single compression test: **a** stress–strain relationship with peaks of the unloading cycles and **b** damage

Fig. 6 Test result of a single tensile test: **a** stress-crack opening relationship with peaks of unloading cycles and **b** damage
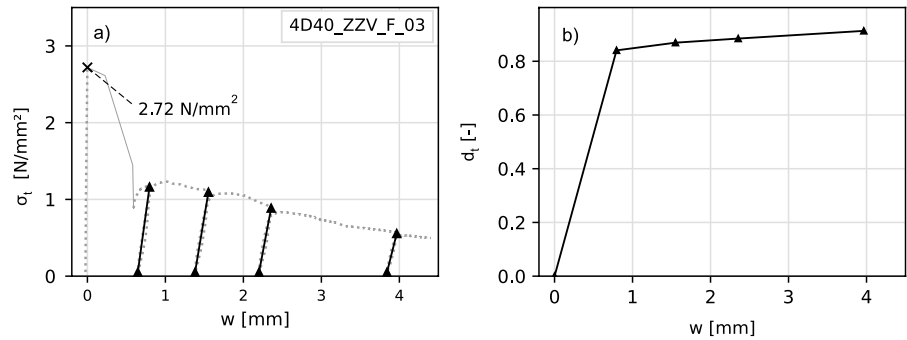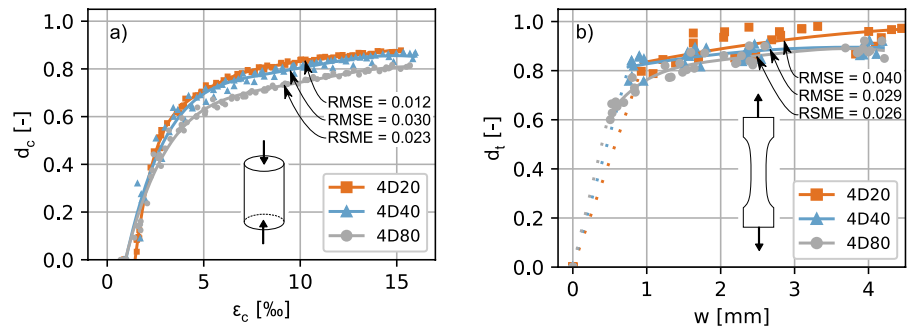

Fig. 7 Damage results of all single tests and with regression polynomials of the series: **a** compression, **b** tension

the same unit as the data, is also reported. The smaller this value, the more accurately the data points are described by the regression polynomial. In the compression tests in Fig. 7a, it can be seen that the data points show little scatter, as reflected in the RMSE between 0.012 and 0.03. The damage curves initially overlap and rise steeply. From a compressive load of around 4‰, the curves flatten out and approach different levels. The curve with a fiber content of 80 kg/m^3, 4D80, exhibits the minimal damage around 0.80. As the fiber content decreases, the damage noticeably increases. The damage reaches a value of 0.88 at a fiber content of 20 kg/m^3 (4D20).

Figure 7b shows the individual values of tensile damage and the corresponding regression curves. Due to the abrupt initial crack opening, it was not possible to collect experimental damage data for very small crack widths. The regression curve is shown dotted up to the first damage result of the respective test series. As can be seen here, increasing fiber content results in less damage for the same crack opening. Again, different final damage levels can be observed, depending on the fiber content. However, the existing scatter is more pronounced

(RMSE from 0.026 to 0.040), which makes it difficult to draw conclusions. The essential result of decreasing final damage levels with increasing SFRC performance is in line with the results from literature [16, 26, 28, 29].

The impact of steel fibers on damage behavior can also be seen in the photos of the compressive specimens themselves. Figure 8 shows cylinders at the end of the low cycle compression test. As (1) the specimens were subjected to loads well in excess of the maximum load and (2) the steel fibers prevent loose parts from breaking off, these fracture patterns should be interpreted in a more qualitative manner. No splitting or shear failures were detected. For comparative purposes, a cylinder without steel fibers is presented on the far left. Some parts of the cylinder are destroyed and are lying beside the rest of the specimen. In contrast, the cylinder with 20 kg/m^3 steel fiber content remains intact despite significant cracking. By increasing the steel fiber content to 40 or 80 kg/m^3, the visible cracks become smaller and smaller. An influence of the steel fibers on the specimen stiffness is therefore obvious.
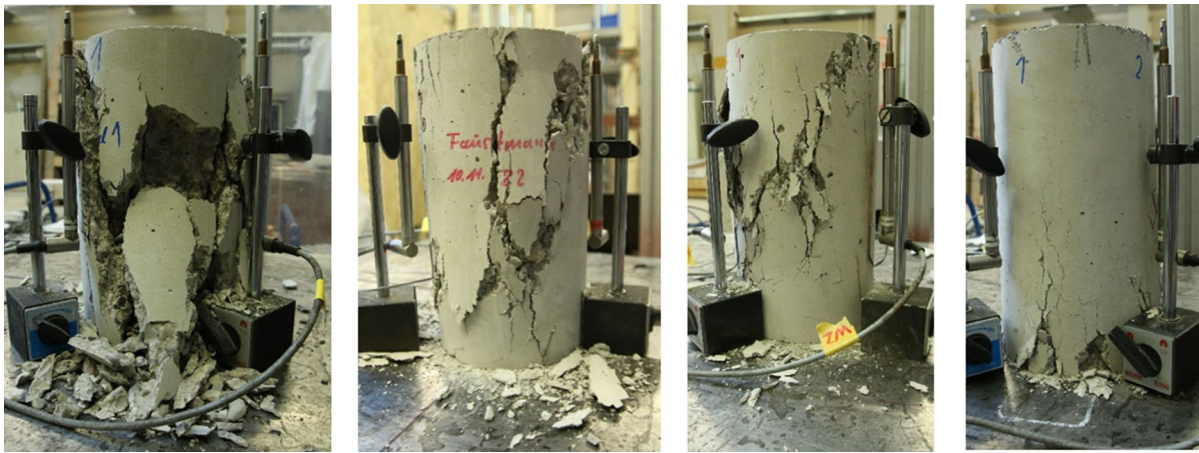
Fig. 8 Cylinders at the end of compression tests with fiber contents (from left to right) of 0.0, 20, 40 and 80 kg/m^3

3 Comparison of the test results with existing damage laws

In this section, the experimental damage data will be compared with the existing damage laws from the literature. We have selected the damage laws of Mark [12], Li [26, 28], and Xu [16] from among known approaches. Below we present a brief overview of them.

Compression and tension damage law according to Mark [12]: In his habilitation thesis [12], Mark formulates damage laws for compression and tension in plain concrete, also published in English in [32]. The existing total strain is divided into the components σ_c / E_{c0} and ε^{in} (see Fig. 4). Subsequently, the damage can be calculated according to Eqs. 3 and 4 as a function of the existing stress σ, the undamaged modulus of elasticity E_{c0} and a control parameter b_c or b_t. Realistic results are obtained with $b_c = 0.70$ and $b_t = 0.10$, according to Mark [12].

Compression damage law according to Mark [12]:

$$d_c = 1 - \frac{\sigma_c/E_{c0}}{\varepsilon_c^{in} \cdot (1 - b_c) + \sigma_c/E_{c0}} \qquad (3)$$

Tension damage law according to Mark [12]:

$$d_t = 1 - \frac{\sigma_t/E_{c0}}{\varepsilon_t^{in} \cdot (1 - b_t) + \sigma_t/E_{c0}} \qquad (4)$$

Compression damage law [26] and tension damage law [28] according to Li: In 2017, Li [26] investigates the compression damage behavior of SFRC with fiber contents of 80–160 kg/m^3. Based on experiments on prisms, Li [26] formulates an empirical damage law, which includes the reinforcing index λ_{sf}. This reinforcing index λ_{sf} is a parameter for describing the performance of the steel fibers, which is calculated from the steel fiber content V_f (volume fraction) of and multiplied by the fiber aspect ratio (Eq. 5). The remaining coefficients in Eq. 6 have been determined empirically by curve fitting. The compressive damage d_c is calculated as a function of the reinforcing index λ_{sf} and the compressive strain ε in ‰. The present stresses are not taken into account.

Compression damage law according to Li [26]:

$$\lambda_{sf} = V_f \cdot \left(\frac{l_f}{d_f} \right) \qquad (5)$$

$$d_c = 1 - (0.627 + 0.088 \cdot \lambda_{sf}) \cdot \varepsilon^{0.173 \cdot \lambda_{sf} - 0.861} \qquad (6)$$

Tension damage law according to Li [28]: Analogous to the above investigations, Li [28] is conducting investigations on the tensile damage behavior of steel fiber concretes with fiber contents of 40–160 kg/m^3. The research manly focused on fiber contents of 120 kg/m^3. Cylindrical specimens with a diameter of 75 mm and a height of 200 mm were used. In addition to the fiber content, the fiber length was

varied between 20 and 40 mm and thus also the fiber slenderness changed. As with the compression damage law ([26]), the reinforcement index according to Eq. (5) is included in the tensile damage law. This is denoted RI in [28], but is still referred to as λ_{sf} here for consistency. Equation 7 shows the tensile damage law according to [28]. In addition to the reinforcement index, the strain ε in μm/m and various empirical factors are included in the model. The present stress is not taken into account.

$$d_t = \left(1 - 0.226 \cdot \lambda_{\text{sf}}\right) + \left(-1.0 + 0.238 \cdot \lambda_{\text{sf}}\right) \cdot e^{-\left(0.001 + 0.242 \cdot e^{-10 \cdot \lambda_{\text{sf}}}\right) \cdot \varepsilon} \tag{7}$$

Compression and tension damage law according to Xu [16]: Xu [16] studies the damage behavior of hybrid fiber concretes containing 80–160 kg/m^3 corrugated steel fibers as well as polypropylene (PP) fibers. Both compression prisms (150/150/300 mm) and tension cylinders (75/200 mm) are cyclically loaded and the damage behavior is analyzed. Equation 8 shows the developed equation to predict the compressive damage of hybrid fiber reinforced concrete. As in Li [26, 28], the reinforcement index λ_{sf} is used in the calculation according to Eq. (5). In addition, a coefficient λ_{pf} is added in the exponent to account for the PP fibers. Neglecting this part, Eq. 9 is obtained.

$$d_c = 0.942 - e^{0.5 \cdot \left(0.2517 \cdot \lambda_{\text{sf}} + 0.3 \cdot \lambda_{\text{pf}} - 1\right) \cdot \varepsilon_c} \tag{8}$$

$$d_c = 0.942 - e^{0.5 \cdot \left(0.2517 \cdot \lambda_{\text{sf}} - 1\right) \cdot \varepsilon_c} \tag{9}$$

For the tensile damage, the approach according to Li [28] also provides applicable results for the hybrid fiber-reinforced cylinders of Xu [16], so that Xu [16] again classifies this approach as applicable and re-publishes it. According to Xu [16], the PP fibers

have no significant influence on the tensile damage behavior.

Comparison of damage laws with experimental results Figure 9 displays a comparison between all the damage laws presented and the experimental damage values for compression and tension in the 4D40 series. This series was selected as its steel fiber content of 40 kg/m^3 is representative of SFRC in Europe [30]. For the compressive damage in Fig. 9a, it can be seen that the approaches according to Xu [16] and Li [26] do not provide agreement with the experimental results, which is reflected by an RMSE of about 0.16 for both models. The damage increases too steeply at low strains and also yields too high damage values for large strains. In contrast, the Mark approach demonstrates very good agreement with the experimental data until a strain of 4 ‰. However, beyond this point, the Mark approach [12] displays an increasing damage level of 0.96, whereas the experimental data remain stagnant at 0.86. The average error RMSE is 0.087.

The comparison of the tensile damage is shown in Fig. 9b). The transfer between crack width and strain is done by the well-known approach $\varepsilon = w/l_c$, (e.g. [1, 47]). The characteristic length l_c, refers to the measurement length of the LVDT's of 130 mm (see Fig. 3), which is very close to the standard value of 125 mm in the next generation of Eurocode 2 [1]. No valid experimental data are available at the initial crack opening (blue dotted line). According to Xu [16], Li [28], and Mark [12], the damage increases rapidly here. At a crack opening of 0.75 mm, at which valid measurement data are available, a large deviation is already evident. The damage laws have all already reached their respective maximum value, while the measurement data still show a clear increase in damage. Between crack widths of 1.0 and 4.0 mm,

Fig. 9 Comparison of damage from series 4D40 with damage laws from literature for **a** compression and **b** tension
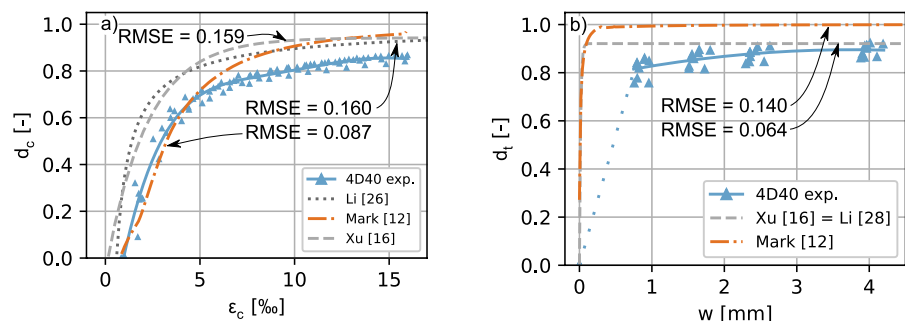
damage increases gradually up to approximately 0.90, which roughly corresponds to the damage for large crack widths according to Xu [16] and Li [28], resulting in a relatively small RMSE of 0.064.

In summary, none of the considered damage laws for compression and tension provides accurate results for typical SFRC. For compressive damage, the approach according to Mark [12] (developed for plain concrete) shows the best results, but for large strains, the damage of the SFRC is overestimated.

4 Enhanced damage law for SFRC

4.1 Development and calibration

In this section, a new/modified damage law will be derived that is capable of representing the experimental damage with sufficient accuracy. It is based on the approach of Mark [12], which is well suited due to its mechanical input values and its easy calibration via the control parameters b_c and b_t. As mentioned in the previous section, especially the damage at very large strains or crack openings differs between the Mark approach and the experiments. While in the Mark approach [12] the damage tends to 1.0, the experimental investigations show a decreasing final damage level with increasing performance of the SFRC. However, this performance depends not only on the steel fiber content, but also on parameters not varied here, such as the fiber type (slenderness, strength, type of anchorage) and the concrete mix [48]. In order to capture the influences of all these parameters, the performance in current codes such as the next generation of Eurocode 2 or Model Code 2010 [1, 47] is therefore described by the mechanical properties achieved, the residual post-crack flexural tensile strengths f_{R1} to f_{R4} in the 3-point flexural test according to EN 14651 [36]. For calculations with "large" crack openings, the f_{R3} value is usually used, which describes the absorbable bending stress at a crack mouth opening displacement of 2.50 mm.

Mark's [12] damage laws are modified so that the final damage level is correctly reflected as a function of the residual flexural tensile strength f_{R3}. To do this, the existing damage laws are multiplied by a term that includes empirical determined constant values in addition to the mechanical material property f_{R3}.

If f_{R3} is set to zero for plain concrete, the multiplicative term is 1.0. The approach thus reduces to Mark's basic formula from [12]. For increasing f_{R3} values, the multiplicative factors are less than 1.0, resulting in a decreasing final damage level. The control parameters b_c and b_t provided by Mark [12] are used to calibrate the curvature of calculated damage. Equations 10 and 11 show the damage laws found.

Developed compression damage law (modified from Mark [12]):

$$d_c = \left(1 - \frac{\sigma_c/E_{c0}}{\varepsilon_c^{\text{in}} \cdot \left(1 - b_c \right) + \sigma_c/E_{c0}} \right) \cdot \left(1 - \frac{f_{R3}}{13 + 5 \cdot f_{R3}} \right)$$
(10)

with $b_c = 0.55$.

Developed tension damage law (modified from Mark [12]):

$$d_t = \left(1 - \frac{\sigma_c/E_{c0}}{\varepsilon_c^{in} \cdot \left(1 - b_t \right) + \sigma_c/E_{c0}} \right) \cdot \left(1 - \frac{f_{R3}}{40 + 3 \cdot f_{R3}} \right)$$
(11)

with $b_t = 0.955$.

Figure 10 shows the comparison of the experimental compressive and tensile damage with the corresponding developed damage law. For the compressive damage in Fig. 10a, a very good agreement between experiment and model can be observed for all concretes tested. Finally, the different final damage levels are now accurately captured. The good agreement between the experimental data and the model is reflected in RMSE values between 0.030 and 0.037, which is only slightly higher than the scatter of the experiments (see Fig. 7a, RMSE between 0.012 and 0.030). The tensile damage in Fig. 10b shows smaller deviations in the range between 0 and 0.5 mm crack opening. It should be noted that no valid experimental data are available in this range. There is also good agreement for crack openings above 0.50 mm. Again, the RMSE values from 0.034 to 0.044 are very close to the experimental scatter (see Fig. 7b, RMSE 0.026 to 0.040). Thus, the developed damage laws for compression and tension have been successfully calibrated.

Fig. 10 Comparison of damage from all test series with the developed damage law developed for **a** compression and **b** tension
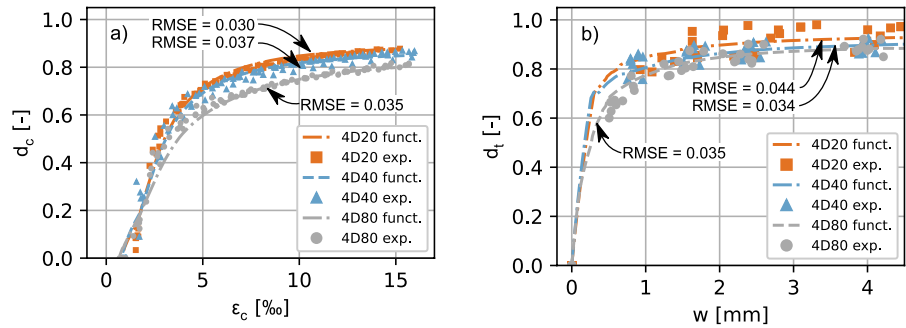

4.2 Parametric study

This section presents the influencing parameters of the model and their effect on the calculated damage. The residual flexural strength f_{R3} is introduced into the model as the significant new parameter. Figure 11a shows the effect of f_{R3} on the calculated compressive damage and Fig. 11b illustrates the effect on the calculated tensile damage. It can be seen that the final damage level is significantly affected at large strains or crack openings. For $f_{R3}=0$, the curves asymptotically approach a limit value of 1.0, as suggested in Mark's initial model [12]. As f_{R3} increases, the final damage level decreases. For an f_{R3} value of 10 N/mm^2, the damage curves approach a limit value of 0.84 in compression and 0.86 in tension.

Figures 11c, 11d show the influence of the control parameters b_c and b_t. The curvature of the damage graph is mainly determined by these parameters. Small values of b_c and b_t result in a rapid increase in damage, while larger values result in smoother curves. However, regardless of the control parameters, the curves tend to have the same final damage level for large strains or crack openings.

Fig. 11 Parameter variation on developed damage law **a** f_{R3} in compression, **b** f_{R3} in tension, **c** control parameter b_c in compression, **d** control parameter b_t in tension
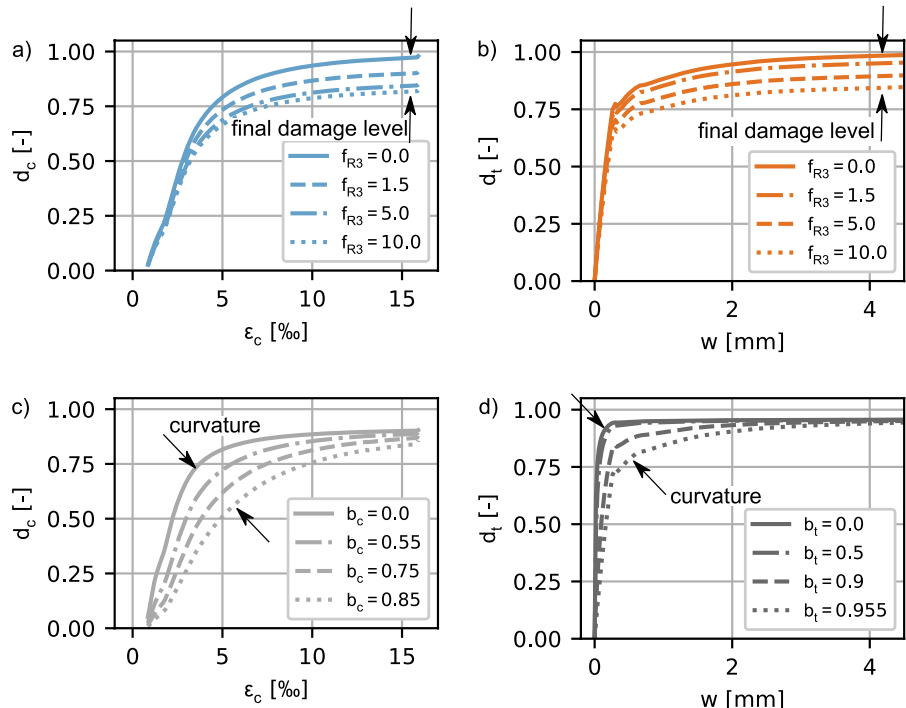
4.3 Application to selected experiments from literature

To further verify the suitability of the damage law, its results are compared with selected test data from the literature. A compression test and a tensile test according to Li [26, 28] were chosen. Neither the modulus of elasticity nor the residual flexural strength f_{R3} are given for these tests. These are required as input values for the application of the damage law, and must therefore calculated using fib Model Code 1990 [37] and the empirical model according to Oettel et. al [48]. This procedure introduces further model uncertainties into the assessment, but due to the lack of data, there is no alternative. We are aware of only one single test where the documented results can be used to analyze the damage and where the residual flexural strength f_{R3} is given. This is test 1.2 by Zhao et al. [49], conducted as a reference test for uniaxial tensile creep tests on SFRC. The modulus of elasticity E_{c0} is also unknown here and was calculated according to fib Model Code 1990 [37]. Table 4 describes the experiments and the input data used for the damage law.

Figure 12 shows a comparison of the experimentally determined damage from the literature as orange dots with the curves determined by calculation using the damage law. Figure 12 a shows the compression test SFB10 from [26]. The blue curve matches the experimental damage qualitatively, but is too low in total. The final damage level from the SFB10 test of approximately $d_t = 0.91$

is underestimated. The deviation is reflected in an higher RMSE value of 0.123.

In [28], Li does not give a crack opening w for the HM10 tensile test, but rather tensile strains. The conversion of the LVDT's readings to strains is not clearly described, so the tensile stress is also plotted against the tensile strains in Fig. 12b. With the control parameter $b_t = 0.955$ calibrated using our own experiments, the calculated damage progression is flatter than stated by Li [28]. However, an adjustment of the control parameter to $b_t = 0.85$ shows very good agreement between the model and the experiment both in the initial range and at the final damage level, resulting in a RMSE of 0.047. The comparison in Fig. 12 c shows a similar result. With a control parameter $b_t = 0.955$ the damage curve is flatter than in test 1.2 of Zhao et al. [49]. However, by adjusting the control parameter to $b_t = 0.65$, very good agreement can be achieved (RMSE = 0.049). The final damage level is well predicted by the model.

5 Discussion

For our own tests, with three series each of compression and tensile tests and a total of 47 specimens, there is very good agreement between the damage determined experimentally and by calculation. This is reflected in RMSE values between 0.030 and 0.044, which is only slightly higher than the experimental RMSE between 0.012 and 0.040. The different final damage levels of the test series

Table 4 Selected damage test from literature for further model validation

| Test from literature | Load/ specimen | V_f (kg/m^3) | Fibers | | | Mechanical properties | | |
			Type	Length l_f (mm)	Aspect ratio l_f/d_f (–)	f_{cm} (N/mm^2)	E_{c0} (N/mm^2)	f_{R3} (N/mm^2)
SFB10 [26]	Compression/ cylinder	80	Corrugated	40	60	37.80	33,479*	6.0**
HM10 [28]	Tension/ cylinder	80	hooked	30	60	51.92	37,248*	7.8**
Test 1.2 [49]	Tension/ notched cylinder	80	hooked	60	65	45	35,496*	6.59

*Value not given in the reference, calculated according to Model Code 1990 [37] with formula: $E_{c0} = 2.15 \cdot 10{,}000 \cdot (f_{cm}/10)^{1/3}$

**Value not given in the reference, calculated according to empirical model by Oettel et. al[48]

Fig. 12 Comparison of selected damage tests from literature with the developed damage law for **a** compression and **b**, **c** tension
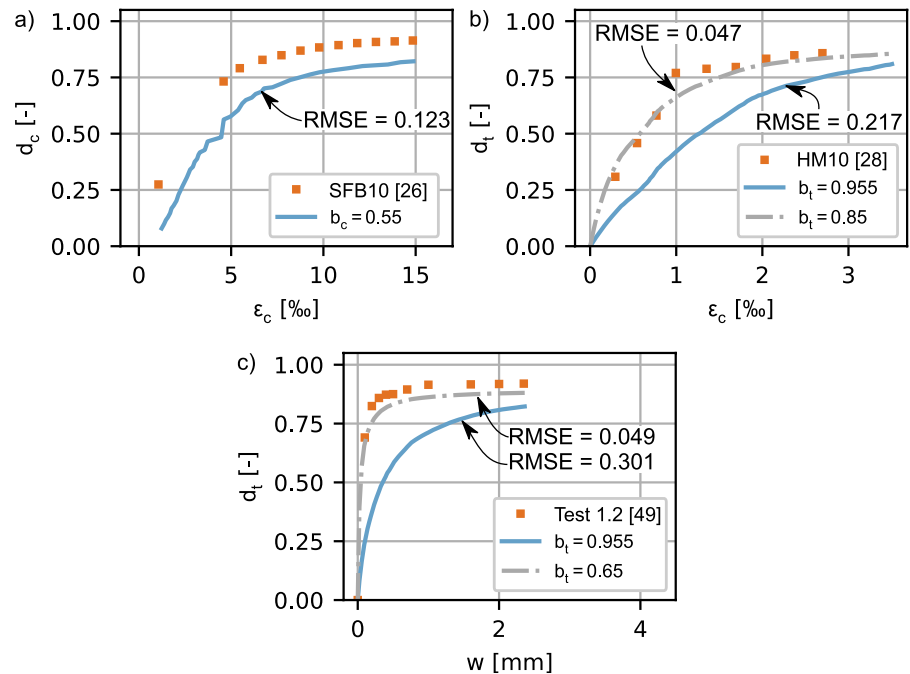
are well covered. For each of the control parameters b_c and b_t, a constant value was found which predicts the damage curve well. Only the steel fiber content was varied in the experiments, the concrete mix design and steel fiber type remained constant. To check the sensitivity and flexibility of the damage law, the essential parameter f_{R3} and the control parameters b_c and b_t were varied. The control parameter in particular allows the curvature of the curve to be flexibly adjusted. Verification of the damage law using test results from the literature proved difficult, particularly as the residual flexural strength f_{R3} and modulus of elasticity E_{c0} are usually not documented. As a workaround, these values were calculated using prediction formulae, which introduces further uncertainty into the comparison.

The need to adjust this final damage level to values less than 1.0 is generally confirmed. The predicted final damage level of the two tensile tests matches the experimental values well, while it is underestimated in the chosen compression test. By adjusting the control parameters b_t, the curves of the two tensile damage tests can be reproduced very well with RMSE less than 0.05. In addition to inaccuracies in the model, the deviations may also be due to a different type of steel fiber (e.g. corrugated), the prediction of f_{R3} and E_{c0}, deviations in the test set-up and

evaluation, and experimental scatter. In particular, the influences of altered concrete mix designs and steel fiber types should be investigated more in detail in the future.

6 Conclusion

Investigations of the damage behavior of plain concrete, SFRC, UHPC and UHSFRC have been the subject of research for many years. This is of great importance for understanding the material behavior, calculating its stiffness and accurately modeling the material properties, e.g. in nonlinear FEM analyses. The present paper presents experiments on typical steel fiber concretes (C30/37, fiber contents about 40 kg/m^3) with modern, end-anchored macro steel fibers, which are becoming increasingly important in Europe. Our experiments focused on compression cylinders and tensile bone specimens to investigate the damage behavior of these concretes. We draw the following conclusions:

1. The damage behavior in compression and tension depends on the performance of the steel fiber concrete. Increasing performance leads to slower

damage development and less damage when experiencing very large strains or crack openings.

2. Existing damage laws are insufficient to accurately describe the experimentally determined damage behavior of SFRC. One possible reason for this weakness is that damage laws from literature were developed on the basis of experiments on plain concrete, hybrid fiber concrete, and steel fiber concrete with very high fiber contents (80 to 160 kg/m^2) rather than common SFRC (C30/37, fiber contents about 40 kg/m^3) which were used in the new experimental studies.

3. We developed a enhanced damage law, based on Mark's damage law [12, 32], to accurately represent the damage resulting from the experiments. We introduced a multiplier to reduce the final damage level depending on the performance of the steel fiber concrete (described by the residual flexural strength according to Model Code 2010 and EN 14651 [36, 47]). In addition, we calibrated the control parameters of Mark b_c and b_t for our SFRC (C30/37 with Dramix 4D 35/65 steel fibers in 20, 40, and 80 kg/m^3).

4. Application of the damage law to test data from the Literature confirms the basic capability of the model. However, the necessary input data for the damage law is often lacking. The control parameters b_c and b_t allow to adapt the predicted damage progression to the results of damage tests on other SFRCs from the literature.

The database of the damage tests should be expanded in order to quantify the influence of factors such as steel fiber type or concrete strength on the damage progression. Based on this, a generally applicable approach for determining the control parameters b_c and b_t could be developed. Future studies should focus on optimizing the experimental setup of the direct tensile tests for very small crack openings. In addition, analyses of the stress-crack-opening relationships in conjunction with the existing fiber orientations, which were not included in this paper, are of further interest.

Author contributions **Sören Faustmann:** Conceptualization, Methodology, Investigation, Writing–original draft, Visualization. **Andreas Wolf**: Investigation (conducting experiments), Data Curation (data evaluation). **Oliver Fischer:** Supervision, Project administration, Writing–review and editing.

Declarations

References

1. European Committee for Standardization (CEN) (2023) Eurocode 2 - Design of concrete structures - Part 1–1: General rules and rules for buildings, bridges and civil engineering structures, FprEN 1992–1–1/2023–04. Brussels.

2. Barros J, Sanz B, Kabele P et al (2020) Blind competition on the numerical simulation of steel-fiber-reinforced concrete beams failing in shear. Struct Concr 2020:1–29. https://doi.org/10.1002/suco.202000345

3. Barros J, Sanz B, Filho M et al (2023) Blind competition on the numerical simulation of continuous shallow steel-fiber reinforced concrete beams failing in bending. Struct Concr 24(3):3877–3907. https://doi.org/10.1002/suco.202200754

4. Schramm N, Fischer O (2016) Investigations on the shear behavior of bridge girders made of normal and ultra-high performance fiber-reinforced concrete. Procedia Eng 156(1):411–418. https://doi.org/10.1016/j.proeng.2016.08.315

5. Sinha BP, Gerstle KH, Tulin LG (1964) Stress-strain relations for concrete under cyclic loading. J American Conc Inst 61(195):211. https://doi.org/10.14359/7775

6. Bahn BY, Hsu CT (1998) Stress-strain behavior of concrete under cyclic loading. ACI Mater J 95:178–193. https://doi.org/10.14359/363

7. Li Z, Peng Z, Teng J et al (2016) Experimental study of damage evolution in circular stirrup-confined concrete. Materials 9(278):1–19. https://doi.org/10.3390/ma9040278

8. Reinhardt HW, Cornelissen HAW (1984) Post-peak cyclic behaviour of concrete in uniaxial tensile and alternating tensile and compressive loading. Cem Concr Res

14(2):263–270. https://doi.org/10.1016/0008-8846(84)90113-3

9. Reinhardt HW, Cornelissen HAW, Hordijk DA (1986) Tensile tests and failure analysis of concrete. J Struct Eng 112(11):2462–2477. https://doi.org/10.1061/(ASCE)0733-9445(1986)112:11(2462)

10. Yankelevsky DZ, Reinhardt HW (1987) Response of plain concrete to cyclic tension. ACI Mater J 84:365–373. https://doi.org/10.14359/1610

11. Hordijk D (1992) Tensile and tensile fatigue behaviour of concrete experiments modelling and analysis. Heron 37:1–79

12. Mark P (2006) Zweiachsig durch Biegung und Querkräfte beanspruchte Stahlbetonträger [Reinforced concrete beams subjected to biaxial bending and shear forces]. Ruhr Universität Bochum (Germany), Shaker Verlag (Aachen), Habilitation

13. Elmorsi M, Kianoush MR, Tso WK (1998) Nonlinear analysis of cyclically loaded reinforced concrete structures. ACI Struct J 95:728–738. https://doi.org/10.14359/586

14. Aslani F, Jowkarmeimandi R (2012) Stress–strain model for concrete under cyclic loading. Mag Concr Res 64(8):673–685. https://doi.org/10.1680/macr.11.00120

15. Dabbagh H, Aslani F (2009) A Comparative Study on the Cyclic Constitutive Models of Concrete. In: 4th International Conference on Construction Materials: Performance, Innovations and Structural Implications: 163 170 https://doi.org/10.13140/2.1.1893.6640

16. Xu L, Wei C, Li B (2018) Damage evolution of steel-polypropylene hybrid fiber reinforced concrete: experimental and numerical investigation. Adv Mater Sci Eng 2018:1–23. https://doi.org/10.1155/2018/1719427

17. Deng F, Chi Y, Xu L et al (2021) Constitutive behavior of hybrid fiber reinforced concrete subject to uniaxial cyclic tension: Experimental study and analytical modeling. Constr Build Mater 295(123650):1–23. https://doi.org/10.1016/j.conbuildmat.2021.123650

18. Wu H, Zhu Z, Chen Y et al (2023) Mechanical properties of short polypropylene fiber enhanced recycled concrete under cyclic compression. Struct Concr 24(4):4751–4766. https://doi.org/10.1002/suco.202300182

19. Krahl PA, Carrazedo R, El Debs MK (2018) Mechanical damage evolution in UHPFRC: experimental and numerical investigation. Eng Struct 170:63–77. https://doi.org/10.1016/j.engstruct.2018.05.064

20. Boulekbache B, Hamrat M, Chemrouk M et al (2016) Flexural behaviour of steel fibre-reinforced concrete under cyclic loading. Constr Build Mater 126:253–262. https://doi.org/10.1016/j.conbuildmat.2016.09.035

21. De Smedt M, Vrijdaghs R, Van Steen C et al (2020) Damage analysis in steel fibre reinforced concrete under monotonic and cyclic bending by means of acoustic emission monitoring. Cement Concr Compos 114(103765):1–13. https://doi.org/10.1016/j.cemconcomp.2020.103765

22. Gebuhr G, Pise M, Anders S et al (2022) Damage evolution of steel fibre-reinforced high-performance concrete in low-cycle flexural fatigue: numerical modeling and experimental validation. Materials 15(1179):1–18. https://doi.org/10.3390/ma15031179

23. Gudžulic V, Neu GE, Gebuhr G et al (2019) Numerisches mehrebenen-modell für stahlfaserbeton: von der faser- zur bauteilebene [numerical multi-level model for steel fibre concrete: from fibre to structural component level]. Beton- und Stahlbetonbau 115(2):146–157. https://doi.org/10.1002/best.201900067

24. Pise M, Brands D, Schröder J et al (2023) Phenomenological material model for damage in steel-fiber reinforced high performance concrete during low cycle fatigue. PAMM 22(1):1–6. https://doi.org/10.1002/pamm.202200236

25. Amziane S, Loukili A (1999) Experimental study of static and cyclic behaviour of steel fibre reinforced high performance concrete. Mater Struct 32:348–353

26. Li B, Xu L, Chi Y et al (2017) Experimental investigation on the stress-strain behavior of steel fiber reinforced concrete subjected to uniaxial cyclic compression. Constr Build Mater 140:109–118. https://doi.org/10.1016/j.conbuildmat.2017.02.094

27. Stamm M (2002) Schädigungsevolution von stahlfaserbeton - schädigungsmechanische simulationsmodelle unter besonderer berücksichtigung der dehnrate [damage evolution of steel fibre reinforced concrete - damage mechanical simulation models with special consideration of the strain rate]. Beton- und Stahlbetonbau 97(7):365–370. https://doi.org/10.1002/best.200201660

28. Li B, Chi Y, Xu L et al (2018) Cyclic tensile behavior of SFRC: Experimental research and analytical model. Constr Build Mater 190:1236–1250. https://doi.org/10.1016/j.conbuildmat.2018.09.140

29. De Smedt M, Vandecruys E, Vrijdaghs R et al (2022) Acoustic emission-based damage analysis of steel fibre reinforced concrete in progressive cyclic uniaxial tension tests. Constr Build Mater 321(126254):1–14. https://doi.org/10.1016/j.conbuildmat.2021.126254

30. Look K, Landler L, Mark P et al (2021) Fasermengen und Leistungsklassen [Fibre quantities and performance classes]. Beton- und Stahlbetonbau 116(S1):13–23. https://doi.org/10.1002/best.202100004

31. Al-Damad IMA, Foster SJ (2022) Behavior of Postcracked steel fiber-reinforced concrete in fatigue and development of a damage prediction model. Struct Concr 23(3):1593–1610. https://doi.org/10.1002/suco.202100497

32. V. Birtel PM Parameterised finite element modelling of RC beam shear failure. In: ABAQUS users' conference, 2006. Online:https://www.researchgate.net/publication/266411260_Parameterised_Finite_Element_Modelling_of_RC_Beam_Shear_Failure. Accessed 15 Mai 2024

33. Bekaert (2023) Dramix 4D 65/35BG datasheet. https://www.bekaert.com/en/product-catalog/content/dop/dramix-4d-technical-documents. Accessed 15 Mai 2024

34. Deutscher Ausschuss für Stahlbeton (2021) DAfStb-richtlinie stahlfaserbeton [guideline for steel fibre reinforced concrete]. Beuth, Berlin

35. DIN EN 12390–13:2021–09 (2021) Prüfung von Festbeton - Teil 13: Bestimmung des Elastizitätsmoduls unter Druckbelastung (Sekantenmodul) [Testing hardened concrete - Part 13: Determination of secant modulus of elasticity in compression; German version EN 12390–13:2021]. https://doi.org/10.31030/3240156

36. European Committee for Standardization (CEN) (2007) EN14651:2005+A1:2007 Test method for metallic fibre concrete - Measuring the flexural tensile strength (limit or proportionality (LOP), residual). Brussels

37. fib (1993) Ceb-Fip Model Code 1990: Design Code; Eton, Comite Euro-International Du Beton.

38. Müller C (2015) Last-Verformungsverhalten zentrisch beanspruchter Stahlbetondruckglieder mit Kreisquerschnitt [Load-deformation behaviour of centrally loaded reinforced concrete compression members with circular cross-section], Dissertation, Technische Universität Carolo-Wilhelmina zu Braunschweig

39. Wille K, El-Tawil S, Naaman AE (2014) Properties of strain hardening ultra high performance fiber reinforced concrete (UHP-FRC) under direct tensile loading. Cement Concr Compos 48:53–66. https://doi.org/10.1016/j.cemconcomp.2013.12.015

40. Amin A, Markić T, Kaufmann W (2019) Direct tension testing of SFRC - Some peculiar effects of the end restraints. In: Proceedings of the 10th International Conference on Fracture Mechanics of Concrete and Concrete Structures. IA-FraMCoS 1 9 https://doi.org/10.21012/fc10.233584

41. Rutzen M, Lauff P, Niedermeier R et al (2021) Influence of fiber alignment on pseudoductility and microcracking in a cementitious carbon fiber composite material. Mater Struct 54(58):1–21. https://doi.org/10.1617/s11527-021-01649-2

42. Look K, Mark P (2022) Steel fiber reinforced concrete tensile testing with eliminated lateral wall effect. Struct Concr 23(6):3483–3496. https://doi.org/10.1002/suco.202100831

43. Zaydowicz K (2023) Stahlfasern ersetzen Bewehrung – Gesteuerte Ausrichtung großer Fasermengen [Steel fibres replace reinforcement - Controlled alignment of large quantities of fibres], Dissertation, Ruhr-Universität Bochum

44. Carrillo J, Pincheira JA, Abellan-Garcia J (2022) Direct tension tests of concrete reinforced with hooked steel fibers. ACI Struct J. https://doi.org/10.14359/51737186

45. Lubliner J, Oliver J, Oller S et al (1989) A plastic-damage model for concrete. Int J Solids Struct 25(3):299–326. https://doi.org/10.1016/0020-7683(89)90050-4

46. Lee J, Fenves GL (1998) Plastic-damage model for cyclic loading of concrete structures. J Eng Mech 124(8):892–900. https://doi.org/10.1061/(asce)0733-9399(1998)124:8(892)

47. fib (2013) fib Model Code for Concrete Structures 2010. Fédération Internationale du Béton, Ernst and Sohn, Lusanne. ISBN: 978–3–433–03061–5

48. Oettel V, Schulz M, Lanwer JP (2021) Empirischer Ansatz zur Bestimmung der Nachrissbiegezugfestigkeit [Empirical approach to determine the residual flexural strength]. Beton- und Stahlbetonbau 116(S1):24–35. https://doi.org/10.1002/best.202100002

49. Zhao G, Di Prisco M, Vandewalle L (2015) Experimental investigation on uniaxial tensile creep behavior of cracked steel fiber reinforced concrete. Mater Struct 48(10):3173–3185. https://doi.org/10.1617/s11527-014-0389-1